Pump-to-Stokes relative intensity noise transfer and analytical modeling of mid-infrared silicon Raman lasers

J. Ma[1] and S. Fathpour[1,2,*]

[1] *CREOL, The College of Optics and Photonics, University of Central Florida, Orlando, Florida, 32816, USA*
[2] *Department of Electrical Engineering and Computer Science, University of Central Florida, Orlando, Florida, 32816, USA*
**fathpour@creol.ucf.edu*

Abstract: An analytical model for mid-infrared (mid-IR) silicon Raman lasers (SRLs) is developed. The relative intensity noise (RIN) transfer from the pump to the Stokes in the lasers is also investigated. The analytical model can be used as a versatile and efficient tool for analysis, design and optimization of mid-IR SRLs. It is shown that conversion efficiency of 70% is attainable and the low-frequency RIN transfer may be suppressed to below 1 dB by pumping low-loss waveguides at high intensities.

OCIS codes: (190.5650) Raman effect; (130.0130) Integrated optics devices.

References and links

1. B. Jalali and S. Fathpour, "Silicon photonics," J. Lightwave Technol. **24**(12), 4600–4615 (2006).
2. B. Jalali, V. Raghunathan, R. Shori, S. Fathpour, D. Dimitropoulos, and O. Stafsudd, "Prospects for silicon mid-IR Raman lasers," IEEE J. Sel. Top. Quantum Electron. **12**(6), 1618–1627 (2006).
3. V. Raghunathan, D. Borlaug, R. R. Rice, and B. Jalali, "Demonstration of a Mid-infrared silicon Raman amplifier," Opt. Express **15**(22), 14355–14362 (2007).
4. D. Borlaug, S. Fathpour, and B. Jalali, "Extreme value statistics in silicon photonics," IEEE Photon. J. **1**(1), 33–39 (2009).
5. T. Baehr-Jones, A. Spott, R. Ilic, A. Spott, B. Penkov, W. Asher, and M. Hochberg, "Silicon-on sapphire integrated waveguides for the mid-infrared," Opt. Express **18**(12), 12127–12135 (2010).
6. R. Soref, "Mid-infrared photonics in silicon and germanium," Nat. Photonics **4**(8), 495–497 (2010).
7. X. Liu, R. M. Osgood, Y. A. Vlasov, and W. M. J. Green, "Mid-infrared optical parametric amplifier using silicon nanophotonic waveguides," Nat. Photonics **4**(8), 557–560 (2010).
8. S. Zlatanovic, J. S. Park, S. Moro, J. M. C. Boggio, I. B. Divliansky, N. Alic, S. Mookherjea, and S. Radic, "Mid-infrared wavelength conversion in silicon waveguides using ultracompact telecom-band-derived pump source," Nat. Photonics **4**(8), 561–564 (2010).
9. G. Z. Mashanovich, M. M. Milošević, M. Nedeljkovic, N. Owens, B. Xiong, E. J. Teo, and Y. Hu, "Low loss silicon waveguides for the mid-infrared," Opt. Express **19**(8), 7112–7119 (2011).
10. Z. Cheng, X. Chen, C. Y. Wong, K. Xu, C. K. Y. Fung, Y. M. Chen, and H. K. Tsang, "Mid-infrared grating couplers for silicon-on-sapphire waveguides," IEEE Photon. J. **4**(1), 104–113 (2012).
11. O. Boyraz and B. Jalali, "Demonstration of a silicon Raman laser," Opt. Express **12**(21), 5269–5273 (2004).
12. H. Rong, R. Jones, A. Liu, O. Cohen, D. Hak, A. Fang, and M. Paniccia, "A continuous-wave Raman silicon laser," Nature **433**(7027), 725–728 (2005).
13. A. Liu, L. Liao, and H. Rong, "Recent development in silicon photonics: 2.5 Gb/s silicon optical modulator and silicon Raman laser," Proc. SPIE **5730**, 80–93 (2005).
14. X. Chen, N. C. Panoiu, and R. M. Osgood, "Theory of Raman-mediated pulsed amplification in silicon-wire waveguides," IEEE J. Quantum Electron. **42**(2), 160–170 (2006).
15. M. Krause, R. Draheim, H. Renner, and E. Brinkmeyer, "Cascaded silicon Raman lasers as mid-infrared sources," Electron. Lett. **42**(21), 1224–1225 (2006).
16. M. Krause, H. Renner, and E. Brinkmeyer, "Theory of silicon Raman amplifiers and lasers," in *Silicon Photonics for Telecommunications and Biomedicine*, S. Fathpour and B. Jalali, eds. (CRC Press, 2012), pp.131–200.
17. I. D. Rukhlenko, M. Premaratne, and G. P. Agrawal, "Nonlinear silicon photonics: analytical tools," IEEE J. Sel. Top. Quantum Electron. **16**(1), 200–215 (2010).
18. H. Rong, S. Xu, O. Cohen, O. Raday, M. Lee, V. Sih, and M. Paniccia, "A cascaded silicon Raman laser," Nat. Photonics **2**(3), 170–174 (2008).
19. M. Krause, S. Cierullies, H. Renner, and E. Brinkmeyer, "Pump-to-Stokes RIN transfer in Raman fiber lasers and its impact on the performance of co-pumped Raman amplifiers," Opt. Commun. **260**(2), 656–661 (2006).
20. X. Sang, D. Dimitropoulos, and B. Jalali, "Influence of pump-to-signal RIN transfer on noise figure in silicon Raman amplifiers," IEEE Photon. Technol. Lett. **20**(24), 2021–2023 (2008).

#166138 - $15.00 USD Received 5 Apr 2012; revised 15 Jun 2012; accepted 13 Jul 2012; published 23 Jul 2012

21. I. D. Rukhlenko, I. Udagedara, M. Premaratne, and G. P. Agrawal, "Effect of free carriers on pump-to-signal noise transfer in silicon Raman amplifiers," Opt. Lett. **35**(14), 2343–2345 (2010).
22. X. Liu, X. Sang, B. Yan, K. Wang, C. Yu, and W. Dou, "Influences of pump-to-Stokes RIN transfer on the single order silicon Raman lasers," J. Optoelectron. Adv. Mater. **4**, 1284–1288 (2010).
23. R. Claps, D. Dimitropoulos, V. Raghunathan, Y. Han, and B. Jalali, "Observation of stimulated Raman amplification in silicon waveguides," Opt. Express **11**(15), 1731–1739 (2003).
24. S. Pearl, N. Rotenberg, and H. M. van Driel, "Three-photon absorption in silicon for 2300-3300 nm," Appl. Phys. Lett. **93**(13), 131102 (2008).
25. F. Leplingard, C. Martinelli, S. Borne, L. Lorcy, D. Bayart, F. Castella, P. Chartier, and E. Faou, "Modeling of multiwavelength Raman fiber lasers using a new and fast algorithm," IEEE Photon. Technol. Lett. **16**(12), 2601–2603 (2004).
26. J. Zhou, J. Chen, X. Li, G. Wu, and Y. Wang, "Exact analytical solution for Raman fiber lasers," IEEE Photon. Technol. Lett. **18**(9), 1097–1099 (2006).
27. Z. Qin, X. Zhou, Q. Li, H. Wu, and Z. Zhou, "An improved theoretical model of nth-order cascaded Raman fiber lasers," J. Lightwave Technol. **25**(6), 1555–1560 (2007).
28. S. A. Babin, D. V. Churkin, and E. V. Podivilov, "Intensity interactions in cascades of a two-stage Raman fiber laser," Opt. Commun. **226**(1-6), 329–335 (2003).
29. C. Huang, Z. Cai, C. Ye, H. Xu, and Z. Luo, "Optimization of dual-wavelength cascaded Raman fiber lasers using an analytic approach," Opt. Commun. **272**(2), 414–419 (2007).
30. K. Huang, X. Zhou, Z. Qin, H. Wu, and Z. Zhou, "A novel fast numerical algorithm for cascaded Raman fiber laser using the analytic approximate solution," Opt. Commun. **271**(1), 257–262 (2007).
31. H. Rong, Y.-H. Kuo, S. Xu, A. Liu, R. Jones, M. Paniccia, O. Cohen, and O. Raday, "Monolithic integrated Raman silicon laser," Opt. Express **14**(15), 6705–6712 (2006).

1. Introduction

Silicon is now an established optical material for passive and active integrated optics and optoelectronics in the near-infrared (near-IR) regime [1]. More recently, silicon photonics has been pursued in the 3-5 μm or mid-wave infrared (MWIR or mid-IR) regime with applications in chemical and biological sensing, tissue photoablation, environmental monitoring and free-space communications [2–10]. The key advantage of the mid-IR wavelength range, as compared with near-IR, is the absence of two-photon absorption (TPA) and free-carrier absorption (FCA) at wavelength above ~2.2 μm [2]. Optical Raman amplification at 3.4 μm [3,4], four-wave mixing and parametric amplification at ~2.2 μm [7,8], silicon-on-sapphire (SOS) waveguides at 4.5 μm [5], silicon-on-insulator waveguides at 3.39 μm [9] and SOS gratings couplers at 2.75 μm [10] are some of the recent developments in the emerging field of mid-IR silicon photonics.

SRLs were first demonstrated in the near-IR regime [11,12]. The works were followed by several simulations on Raman lasers and amplifiers [13–17]. The longest wavelength experimentally reported in the near-IR is a cascaded laser operating at 1.848 μm [18]. Cascaded Raman lasers up to 3 μm and pumped at 1.55 μm have been studied based on fully numerical methods [15]. No experimental work on mid-IR SRLs has yet been reported to the best of our knowledge. It is, nonetheless, mentioned that demonstration of 3.4 μm mid-IR SRLs has been attempted by the present authors in mirror-coated 1-inch thick silicon ingots and using a setup similar to that described in Ref [4]. Although spontaneous Raman emission was certainly observed and the bulk device was perhaps at or slightly above threshold, the low average power and the poor beam quality of the employed pump source (VIBRANT IR Model 2731 optical parametric oscillator by OPOTEK, Inc.) prevented definite and undisputable confirmation of lasing. It is our belief that optical waveguiding would alleviate some of these issues provided that low-loss mid-IR silicon waveguides [9] and efficient coupling schemes [10] are simultaneously employed.

This paper reports an analytical model for mid-IR SRLs for the first time. The developed analytical model can be used to avoid time-consuming fully numerical simulations in the design and analysis of the devices. The model is validated by comparing it with numerical solutions of coupled-wave equations, and is used to predict the performance of the lasers.

The Rician distribution of pump amplitude fluctuations has been shown to have a significant impact on the pulse-to-pulse gain statistics of mid-IR Raman amplifiers [4]. Similarly, the RIN transferred from the instability of the pump source to the output Stokes can have a significant impact on the performance of mid-IR SRLs. The RIN transfer has been

#166138 - $15.00 USD Received 5 Apr 2012; revised 15 Jun 2012; accepted 13 Jul 2012; published 23 Jul 2012

theoretically and experimentally studied in Raman fiber lasers [19], and has been numerically simulated in near-IR silicon Raman amplifiers and lasers [20–22]. In this paper, the impact of RIN transfer on the performance of mid-IR SRLs is investigated for the first time.

2. Methodology

There are several nonlinear effects in silicon besides Raman scattering that may influence the performance of SRLs. Necessary assumptions should be made in order to simply the model without any loss of accuracy. Stimulated Brillouin Scattering (SBS) presents a serious problem in Raman fiber lasers (RFLs). However, SBS can be ignored in SRLs as the Brillouin scattering coefficient for silicon is two orders of magnitude smaller than the Raman gain coefficient [23]. Three-photon absorption (3PA) and associated free-carrier effects are also negligible because the corresponding coefficient for silicon is very small [24]. Degenerate four-wave mixing between the pump and the generated Stokes waves can be discarded as the phase matching condition cannot be satisfied due to the large difference of the interacting wavelengths. Therefore, only stimulated Raman scattering (SRS) is considered. This assumption is consistent with previous works on SRLs [13,15,16].

With the absence of TPA and FCA at above 2.2 μm, the coupled-wave equations for Raman lasing lend themselves to analytical solutions, as developed here. This is in contrast to near-IR wavelengths where achieving accurate analytical solutions is difficult, if not impossible, and hence fully numerical simulation are usually employed [13–17]. The model is applicable to various silicon waveguide configurations as well as bulk silicon, coated or uncoated with dielectric or integrated mirrors, provided that the predicted pump intensities are achievable in practice. Figure 1(a) shows the schematic of the SRL analyzed in this work in which the input pump is injected from the left-hand side (LHS) and the output Stokes is from the right-hand side (RHS). As discussed later, a device in which the output is from the LHS was also studied but exhibited very similar performance. In either case, the device consists of a silicon waveguide of length L, whose facets are coated with multilayer dielectric films. A continuous wave (CW) pump laser (p) at wavelength λ_p is coupled into the LHS (l) of the cavity and the output Stokes (s) wavelength λ_s is exited from the RHS (r) via stimulated Raman scattering. The reflectivities of the left and right mirrors at λ_p and λ_s are R_{pl}, R_{pr}, R_{sl} and R_{sr}, respectively.

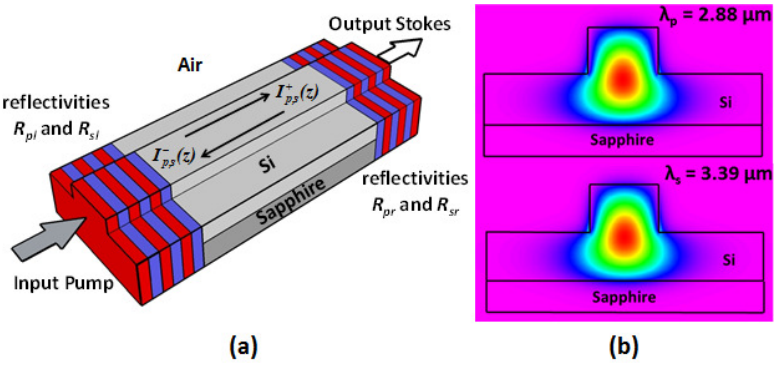

Fig. 1. (a) Schematic of the studied mid-IR silicon Raman laser; (b) Optical mode profile (TE) at pump (top) and the Stokes (bottom) wavelengths in the SOS waveguide with air top-cladding having rib width of 2 μm, rib height of 2 μm and slab height of 1μm. The calculations are obtained from a commercial numerical mode solver (BeamPROP by RSoft).

A typical micron-size ridge waveguide with the geometry described in the caption of Fig. 1 was analyzed. Figure 1(b) shows the TE optical modes propagating in the SOS waveguide at both the pump and the Stokes wavelengths. The effective core area of the waveguide is ~3 μm^2. The overlap of the two modes, Γ, is calculated to be close to unity (99.75%). The overlap integral, Γ, is included in the following model (Eqs. (1) and (2)) for completeness.

#166138 - $15.00 USD Received 5 Apr 2012; revised 15 Jun 2012; accepted 13 Jul 2012; published 23 Jul 2012

However, its value is assumed to be 1 for the present micron-size ridge waveguides. It is noted that Γ could be considerably smaller than unity in submicron waveguides.

As mentioned, TPA and FCA are negligible at mid-IR wavelengths [2]. By also neglecting spontaneous Raman scattering at and above threshold, the evolution of the forward (+) and backward (–) propagating pump and Stokes intensities are governed by the following coupled-wave equations [13]

$$\pm\frac{dI_p^{\pm}}{I_p^{\pm}dz} = -\alpha_p - \Gamma g_R \cdot \frac{\lambda_s}{\lambda_p}(I_s^+ + I_s^-), \tag{1a}$$

$$\pm\frac{dI_s^{\pm}}{I_s^{\pm}dz} = -\alpha_s + \Gamma g_R \cdot (I_p^+ + I_p^-) \tag{1b}$$

where g_R is the Raman gain coefficient, α_p and α_s are the linear propagation losses at λ_p and λ_s, respectively. The corresponding boundary conditions are

$$\begin{aligned} I_p^+(0) &= (1-R_{pl})I_{in} + R_{pl}I_p^-(0), \\ I_p^-(L) &= R_{pr}I_p^+(L), \\ I_s^+(0) &= R_{sl}I_s^-(0), \\ I_s^-(L) &= R_{sr}I_s^+(L), \end{aligned} \tag{2}$$

where I_{in} is the input pump intensity.

Equations (1) and (2) might be considered to be similar to the coupled-wave equations and boundary conditions of near-IR RFLs. Although several analytical and numerical models for RFLs have been published [25–30], each has its own shortcoming for the present case, as follows. F. Leplingard *et al*. simplified the numerical algorithm for solving the equations by transforming the two-point boundary value problem into an initial value problem, but the solution was still fully numerical [25]; The analytical solution developed by J. Zhou *et al*. assumed single pass pump, i.e., anti-reflection coated mirrors [26]; Other analytical models developed for RFLs assume zero left-mirror reflectivity at the pump wavelength (a simplifying valid assumption because of the low index of silica) [27–30]; Z. Qin *et al.* made the further simplifying assumption of zero residual pump power reflected back to the input end [27]; S. A. Babin *et al.* not only assumed zero left-mirror reflectivity but also assumed that the output power increases linearly with the input [28]. However, none of these models are applicable to silicon Raman lasers because a considerable amount of pump power reflects back and forth between the right- and left-hand side mirrors into the cavity. Indeed, a variety of dielectric coated mirrors, with different reflectivities at pump and Stokes wavelengths are commonly considered in silicon Raman lasers. Therefore, in this paper, nonzero left- and right- mirror reflectivities at both pump and Stokes wavelengths are included in the modeling of Raman lasers, for the first time, to account for silicon and other high-index material cases (the simplest example may be uncoated air-silicon interface with reflectivity of ~30% at both pump and Stokes). This will require developing a more complicated mathematical treatment of the problem, as presented here.

The above differential equations with the boundary conditions can be solved numerically by collocation. However, an initial guess is usually required for numerical methods. In our case, this guess is difficult to find because zero Stokes intensity is always a possible solution even when the pump intensity is above lasing threshold. Therefore, an analytical solution to this boundary-value problem is developed. The presented solution can be utilized not only as an initial guess for numerical solvers but also as a fully-analytical model.

First, the geometric mean intensity $\bar{I}_{p,s}^{1/2} = (I_{p,s}^+ I_{p,s}^-)^{1/2}$ and the gain factor $G_{p,s}(z) = 1/2\ln I_{p,s}^+(z)/I_{p,s}^-(z)$ are defined [25–30]. As proved in Appendix A, $\bar{I}_p$ and $\bar{I}_s$

#166138 - $15.00 USD Received 5 Apr 2012; revised 15 Jun 2012; accepted 13 Jul 2012; published 23 Jul 2012

are constant, i.e., they are independent of z. As a result, Eqs. (1) and (2) can then be rewritten in terms of $\bar{I}_{p,s}$ and $G_{p,s}(z)$ (Eqs. (A2)-(A4)). A linear dependence of $G_p(z)$ on z is also assumed, i.e.,

$$G_p(z) = G_p(0) + z[G_p(L) - G_p(0)]/L. \tag{3}$$

This linear assumption implies that the pump depletes exponentially in both forward and backward directions. The validity of this linear dependency assumption was confirmed by comparison with fully numerical solutions (Fig. 2).

Based on the above, the threshold intensity of the silicon Raman laser is obtained as

$$I_{th} = \frac{\alpha\delta_s(1-R_{pl}e^{-2\delta_p})(e^{\delta_p} - R_{pl}e^{-\delta_p})}{g_R(1-R_{pl})(1-e^{-\alpha L})(1+R_{pr}e^{-\alpha L})}, \tag{4}$$

where

$$\delta_p = \alpha L + 1/2\ln(1/R_{pr}), \tag{5a}$$

$$\delta_s = \alpha L + 1/2\ln(1/R_{sl}R_{sr}) \tag{5b}$$

are loss factors of the pump and Stokes waves due to linear propagation loss and mirror transmission losses. A detailed derivation of Eq. (4) is presented in Appendix A. By defining

$$L_{p,s}(z) = L\frac{\sinh[G_{p,s}(z)] - \sinh[G_{p,s}(0)]}{G_{p,s}(L) - G_{p,s}(0)}, \tag{6}$$

above threshold, $\bar{I}_p$ can be solved from

$$\bar{I}_p^{1/2} = \delta_1/[2g_R L_p(L)]. \tag{7}$$

Consequently, the geometric mean intensity and gain factor of the Stokes wave are obtained from

$$\bar{I}_s^{1/2} = \lambda_p[G_p(0) - \delta_0]/[2g_R\lambda_s L_s(L)], \tag{8}$$

$$G_s(z) = G_s(0) - \alpha z + 2g_R\bar{I}_p^{1/2}L_p(z). \tag{9}$$

$G_{p,s}(z)$ and $G_{p,s}(L)$ in Eq. (3) and Eqs. (5)-(7) are easily obtained from Eq. (2). Finally, the intensity distributions for the pump and Stokes wave are

$$I_{p,s}^{\pm}(z) = \bar{I}_{p,s}^{1/2}\exp[\pm G_{p,s}(z)], \tag{10}$$

and the output of the laser at the Stokes wavelength on the RHS of the waveguide in Fig. 1(a) is finally

$$I_{out} = (1-R_{sr})I_s^{+}(L). \tag{11}$$

An equation similar to Eq. (11) can be easily obtained if the laser output beam is at the LHS, i.e., the case where the laser output and input beams are counterpropagating.

Unlike the above model for the light-light characteristics, the governing equations for RIN transfer in SRLs do not lend themselves to analytical solutions. To estimate the effect of RIN transfer from the pump to the Stokes output, the noise component at angular frequency Ω in the pump noise spectrum is considered. The intensity fluctuations of the pump and the Stokes wave, normalized to the average intensities, are represented by $m_p^{\pm}(z)$ and $m_s^{\pm}(z)$, respectively:

#166138 - $15.00 USD Received 5 Apr 2012; revised 15 Jun 2012; accepted 13 Jul 2012; published 23 Jul 2012

$$I_p^{\pm}(z,t) = \bar{I}_p^{\pm}(z)[1 + m_p^{\pm}(z)\exp(i\Omega t)], \tag{12a}$$

$$I_s^{\pm}(z,t) = \bar{I}_s^{\pm}(z)[1 + m_s^{\pm}(z)\exp(i\Omega t)], \tag{12b}$$

where $\bar{I}_p^{\pm}(z)$ and $\bar{I}_s^{\pm}(z)$ are time-independent average intensities. $m_p^{\pm}(z)$, $m_s^{\pm}(z)$ are complex values satisfying $\left|m_p^{\pm}(z)\right|, \left|m_s^{\pm}(z)\right| << 1$. The input pump is assumed to be modulated by a sinusoidal function at angular frequency Ω, i.e., $I_{in} = \bar{I}_{in}[1 + m_{in}\exp(i\Omega t)]$, where m_{in} is a small real number. The different values of pump and Stokes group velocities, v_p and v_s, should be accounted for similar to Raman amplifiers [20,21]. This leads to reduced RIN transfer:

$$\pm\frac{\partial I_p^{\pm}}{\partial z} + \frac{1}{v_p}\frac{\partial I_p^{\pm}}{\partial t} = -\alpha_p I_p^{\pm} - g_R \cdot \frac{\lambda_s}{\lambda_p}(I_s^{+} + I_s^{-})I_p^{\pm}, \tag{13a}$$

$$\pm\frac{\partial I_s^{\pm}}{\partial z} + \frac{1}{v_s}\frac{\partial I_s^{\pm}}{\partial t} = -\alpha_s I_s^{\pm} + g_R \cdot (I_p^{+} + I_p^{-})I_s^{\pm}. \tag{13b}$$

Substituting Eq. (12) into Eqs. (13) and (2) and neglecting higher order fluctuation terms, a total of eight coupled differential equations and eight boundary conditions can be obtained. This is a somewhat more complicated problem compared to the only four [20] or six (to account for carrier density noise [21]) equations and boundary conditions that ought to be solved for silicon Raman amplifiers. The equations for steady state operation and corresponding boundary conditions can be obtained by replacing $I_{p,s}^{\pm}$ in Eqs. (1) and (2) with $\bar{I}_{p,s}^{\pm}$ and solved using the analytical model mentioned above. The other four coupled equations and four boundary conditions that describe the small fluctuations on the pump and Stokes waves along transmission length z are derived as:

$$\frac{dm_p^{\pm}}{dz} = \mp\frac{i\Omega}{v_p}m_p^{\pm} \mp g_R\frac{\lambda_s}{\lambda_p}(\bar{I}_s^{+}m_s^{+} + \bar{I}_s^{-}m_s^{-}), \tag{14a}$$

$$\frac{dm_s^{\pm}}{dz} = \mp\frac{i\Omega}{v_p}m_s^{\pm} \pm g_R(\bar{I}_p^{+}m_p^{+} + \bar{I}_p^{-}m_p^{-}), \tag{14b}$$

$$\begin{aligned} &\bar{I}_p^{+}(0)m_p^{+}(0) = (1 - R_{pl})\bar{I}_{in}m_{in} + R_{pl}\bar{I}_p^{-}(0)m_p^{-}(0), \\ &m_p^{-}(L) = m_p^{+}(L), m_s^{+}(0) = m_s^{-}(0), m_s^{-}(L) = m_s^{+}(L). \end{aligned} \tag{15}$$

Equations (14) and (15), together with the steady-state equations, can be numerically solved using the collocation method, from which the RIN transferred from the pump to the Stokes is calculated as

$$T_{RIN}(\Omega) = \frac{\left|m_s^{+}(L,\Omega)\right|^2}{m_{in}^2}. \tag{16}$$

3. Results and discussion

The above general model was applied to specific examples. In all the following numerical and analytical solutions, a pump wavelength of 2.88 μm is used [3,4]. The corresponding Stokes wavelength is 3.39 μm according to silicon's optical phonon energy. The experimentally estimated Raman gain coefficient g_R of 9 cm/GW at these wavelengths was employed [3].

A non-coated 2-cm long-cavity was first analytically modeled by assuming that reflectivities at both pump and Stokes wavelengths were 30%. Fully numerical simulation to

#166138 - $15.00 USD Received 5 Apr 2012; revised 15 Jun 2012; accepted 13 Jul 2012; published 23 Jul 2012

coupled-wave equations was also carried out for this special case by using the results from the analytical method as guesses for the initial solution. Figure 2(a) presents the comparison between the analytical and numerical solutions. The intensity distributions of the pump and Stokes waves in the laser cavity for an input intensity of I_{in} = 200 MW/cm^2 are plotted using both methods. Such pump intensities can be attained in practice by solid-state mid-IR lasers (e.g., optical parametric oscillators) [3,4]. Also shown in the inset of Fig. 2(a) is the input-output (light-light) characteristic of the laser. It is clearly evident that the results have excellent agreement. The validity of the model was rigorously tested under other boundary condition examples not presented here. Meanwhile, the analytical model is proved to be much faster than the traditional numerical way of solving this set of equations. For example, the time consumed for plotting the inset of Fig. 2(a) is 200 times faster than numerical simulations. Therefore, our analytical model can be confidently used as a convenient and efficient tool in design and optimization of mid-IR SRLs. The results of Fig. 2(a) also suggest that at mid-IR wavelengths, where TPA and FCA are negligible, it is possible to pump a non-coated CW SRL above threshold with a reasonable pump intensity of around 100 MW/cm^2. It is reminded that CW near-IR SRLs are not achievable at any pump intensity without using appropriate mirror coatings on top of employing the carrier sweep-out technique to reduce the carrier lifetime [12].

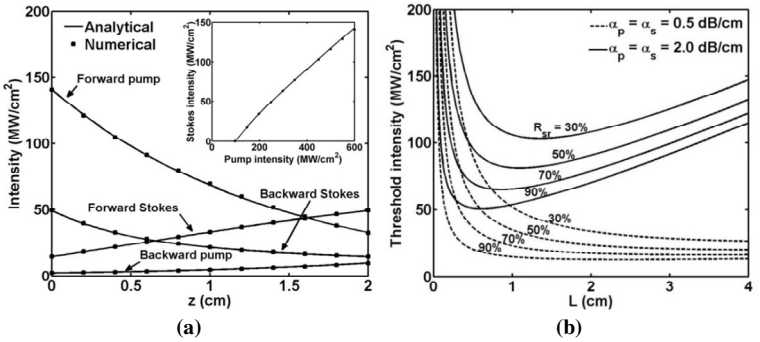

Fig. 2. (a) Intensity distributions of pump and Stokes waves with I_{in} = 200 MW/cm^2. $R_{pl} = R_{pr} = R_{sl} = R_{sr}$ = 30%, $\alpha_p = \alpha_s$ = 0.5 dB/cm and L = 2 cm were assumed. The inset shows the input-output characteristics of the Raman laser. (b) Threshold intensity versus cavity length for various output facet reflectivities and propagation losses and for R_{pl} = 10%, $R_{pr} = R_{sl}$ = 90%.

Using the described analytical model, it is easy to analyze mid-IR SRLs and optimize their design parameters. Indeed, achieving all the following results would have been extremely challenging and time-consuming based on fully numerical models. Figure 2(b) shows the threshold intensity as a function of L for different right facet reflectivities and two different linear propagation losses of 0.5 and 2.0 dB/cm. Unlike near-IR SRLs that have no lasing threshold outside a limited range of lengths [16], mid-IR silicon waveguide cavities can lase for any given length if enough pump power is available. Also, it is evident that for fixed reflectivities, there is an optimum length, where the lasing threshold reaches a minimum. This is more remarkable at the higher studied propagation loss (2.0 dB/cm), as an optimum length of < ~1 cm can be recognized.

Figure 3 shows the influence of the cavity parameters, length and facet reflectivities, on the energy conversion efficiency of the lasers, defined as I_{out}/I_{in}. Generating each 3D plot in Fig. 3 was achieved in about 10 minutes with a typical desktop PC (with a 3 GHz Intel(R) Core(TM)2 Duo CPU), while it can take days to make similar plots based on fully numerical methods. However, our analytical model offers an efficient way to optimize the design of mid-IR SRLs. In this case, L and R_{sr} could be optimized under certain pump intensities. For linear propagation loss of $\alpha_p = \alpha_s$ = 0.5 dB/cm, maximum conversion efficiencies of 55.8% and 45.1% are obtained at input intensities of I_{in} = 200 and 100 MW/cm^2, respectively (Fig. 3(a) and (c)). Such high conversion efficiency have been previously estimated based on fully

#166138 - $15.00 USD Received 5 Apr 2012; revised 15 Jun 2012; accepted 13 Jul 2012; published 23 Jul 2012

numerical simulations and indicate that silicon Raman lasers in the mid-IR can attain performances comparable to near-IR fiber Raman lasers [15]. The lasers' efficiency, however, drop quickly for devices with the higher loss, i.e., $\alpha_p = \alpha_s = 2.0$ dB/cm. The maximum conversion efficiency obtained are 30.5% and 13.5% at input intensities of $I_{in} = 200$ and 100 MW/cm^2, respectively (Fig. 3(b) and (d)). The optimum lengths are below 0.4 cm in these two cases. Further increasing the length will result in higher lasing threshold and lower slope efficiency at the same time. Nonetheless, these predictions indicate a key advantage of mid-IR lasers, as compact laser cavities can be demonstrated. In comparison, up to 5 cm lengths are required at near-IR wavelengths [12]. It is noted that even more compact devices can be envisioned using ring resonator Raman lasers, as reported in the near-IR [31]. However, the study of such lasers is beyond the scope of this work.

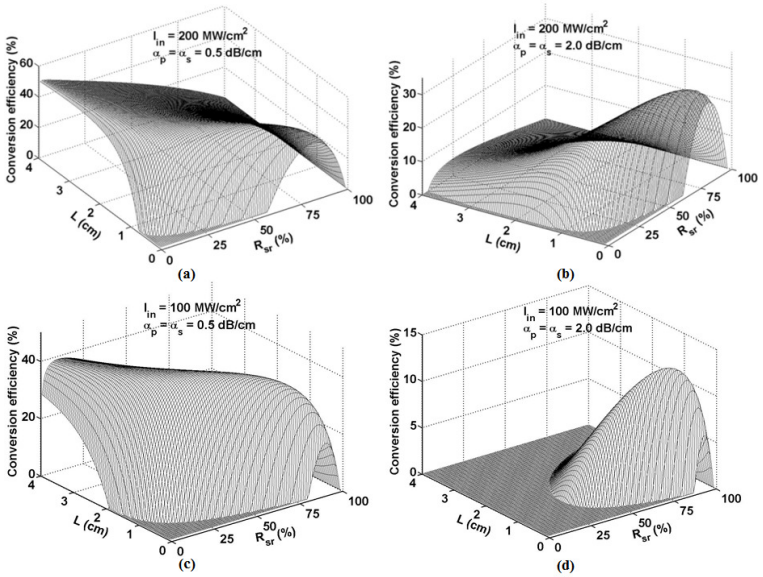

Fig. 3. Conversion efficiency versus cavity length L and output facet reflectivity R_{sr} for two propagation loss values and two pump intensities.

The maximum conversion efficiencies achievable for four propagation loss values are plotted versus pump intensity in Fig. 4. For devices with the lowest loss, i.e., $\alpha_p = \alpha_s = 0.1$ dB/cm, the maximum possible conversion efficiency is ~73%. This could be considered as a practical limit for the efficiency of a mid-IR SRL assuming extremely low-loss silicon waveguides. Pumping the laser with intensities above 200 MW/cm^2 is unnecessary in this case as it could hardly improve the conversion efficiency. For devices with higher loss, i.e., $\alpha_p = \alpha_s = 1.0$ or 2.0 dB/cm, the conversion efficiency has not yet reached saturation at an intensity of 500 MW/cm^2. The minimum achievable lasing thresholds for the four propagation loss values are recognizable by the intersections of the curves with the x-axis.

It is noted that unlike Raman amplifiers whose gain depends on whether a co- or counter-propagating scheme is employed [16], our studies on mid-IR SRLs suggest that there is little dependency of the devices' conversion efficiency on the propagation directions of the pump and the output Stokes wave. This difference between Raman amplifiers and lasers can be attributed to the fact that the asymmetric impact of the nonuniform pump distribution along the waveguide is more pronounced in amplifiers – whose Stokes signal is typically passed a single time through the waveguide – as opposed to lasers whose Stokes output wave experiences several roundtrips in the cavity.

#166138 - $15.00 USD Received 5 Apr 2012; revised 15 Jun 2012; accepted 13 Jul 2012; published 23 Jul 2012

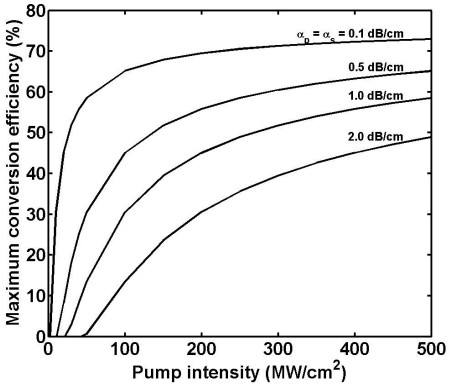

Fig. 4. Maximum conversion efficiency versus pump intensity for four different propagation loss values.

Finally, the RIN transfer in a SRL with a linear waveguide loss of 0.5 dB/cm and for an optimized pump intensity of 100 MW/cm^2, i.e., L = 1.20 cm, R_{sr} = 38% (assuming R_{pl} = 10% and $R_{pr} = R_{sl}$ = 90%), was numerically evaluated. Noise frequencies ranging from zero to tens of gigahertz were included. The group velocity at the pump wavelength in Eqs. (13a) and 14(a) was calculated as $v_p = c/n_{eff}$, where c is the speed of light in vacuum and n_{eff} is the effective index of the silicon waveguide at pump wavelength. The group velocity at the Stokes wavelength was obtained from $v_s = 1/[(\lambda_s - \lambda_p)D + 1/v_p]$, where $D = -120$ ps/(nm.km) is the local group-velocity dispersion in silicon calculated by the Sellmeier equation. This material dispersion dominates the waveguide dispersion in the studied large cross-section waveguides. This was validated by RSoft calculations and is consistent with previous works [20–22]. Finally, m_{in} = 0.01 is assumed in our simulation but even higher values for this quantity changes the following calculations insignificantly.

Figure 5(a) presents the pump-to-Stokes RIN transfer spectrum for pump intensities of 50, 75, 100 and 200 MW/cm^2. It is evident that the RIN transfer remains constant at low frequencies, then starts to oscillate at the free spectral range (FSR) of the laser cavity, i.e., $\Delta\upsilon = c/(2n_{eff} L)$ = 3.6 GHz. The observed strong oscillations at higher frequencies suggest that laser sources with RIN spectra no wider than a few GHz are required for pumping mid-IR lasers with cavity lengths of ~1 cm. The low-frequency transferred RIN, as well as the magnitude of the high-frequency oscillations, drop as the pump power increases. This is consistent with theoretical and experimental RIN transfer spectrum of Raman fiber lasers [19]. The low-frequency RIN transfer for the SRL could be above 12 dB when pumped at 50 MW/cm^2, and drops to below 1 dB at a pump intensity of 200 MW/cm^2.

Results very close to Fig. 5(a) were obtained for the case in which the laser output and the input pump are counterpropagating. This differs from Raman amplifiers that show a higher RIN bandwidth for the copropagation scheme as compared with the counterpropagation scheme [20].

#166138 - $15.00 USD Received 5 Apr 2012; revised 15 Jun 2012; accepted 13 Jul 2012; published 23 Jul 2012

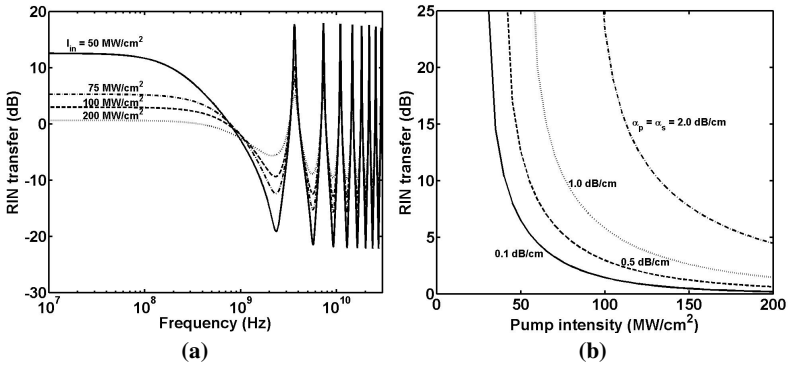

Fig. 5. (a) RIN transfer spectra for mid-IR SRLs pumped at 50, 75, 100 and 200 MW/cm^2 and (b) the devices' low frequency RIN transfer versus pump intensity for four propagation loss values. Modal parameter: L = 1.20 cm, R_{sr} = 38%, α = 0.5 dB/cm (optimized design for I_{in} = 100 MW/cm^2), D = – 120 ps/(nm·km).

Figure 5(b) summarizes the low-frequency RIN transfer versus pump intensity under different propagation loss values. The RIN transfer observed goes to infinity right below the lasing threshold and decreases with increasing pump intensity. Also evident is the noticeable increase in the low-frequency RIN transfer with increasing propagation loss. Unlike near-IR SRLs, in which the RIN transfer is strongly affected by FCA [21], the RIN transfer in mid-IR lasers is mainly determined by the linear propagation loss and the pump intensity. Therefore, pumping at well-above lasing threshold and reducing the linear loss of silicon waveguides are two crucial requirements for decreasing the RIN transfer in mid-IR SRLs.

4. Conclusions

In summary, an analytical model is presented to predict the performance of mid-IR SRLs. The model has excellent agreement with numerical solutions, and hence it can be conveniently used as a versatile design and optimization tool or to find good initial guesses for numerical methods. The effects of cavity parameters on the conversion efficiency of the lasers were studied. The pump-to-Stokes RIN transfer of mid-IR SRLs is also numerically studied. The results show that the low frequency RIN transfer is a strong function of pump intensity and linear propagation loss. For a linear propagation loss of 0.5 dB/cm and a pump intensity of 200 MW/cm^2, the optimized cavity length and output facet reflectivity are 1.04 cm and 22%, respectively. The maximum possible conversion efficiency is ~56%, and the pump-to-Stokes RIN transfer is ~1 dB. For a linear propagation loss of 2.0 dB/cm and same pump intensity, the corresponding values will be 0.34 cm (length), 58% (R_{sr}), 31% (conversion efficiency) and 4 dB (RIN transfer). The results of this study predict strong prospects for mid-IR silicon Raman lasers for high-performance biochemical and communication applications provided that low-noise mid-IR pump sources with high beam-quality and efficient waveguiding schemes exist.

Appendix A

The derivation of the threshold intensity (Eq. (4)) is presented here. The independence of $\bar{I}_p$ and $\bar{I}_s$ on propagation distance z is proved first. Substituting Eq. (1) into $\bar{I}_p^{1/2} = (I_p^+ I_p^-)^{1/2}$ gives

$$\begin{aligned} \frac{d\bar{I}_p}{dz} &= \bar{I}_p^+ \frac{d\bar{I}_p^-}{dz} + \frac{d\bar{I}_p^+}{dz}\bar{I}_p^- \\ &= \bar{I}_p^+ [\alpha_p + g_R \frac{\lambda_s}{\lambda_p}(I_s^+ + I_s^-)]\bar{I}_p^- + [-\alpha_p - g_R \frac{\lambda_s}{\lambda_p}(I_s^+ + I_s^-)]\bar{I}_p^+ \bar{I}_p^- = 0. \end{aligned} \tag{17}$$

#166138 - $15.00 USD Received 5 Apr 2012; revised 15 Jun 2012; accepted 13 Jul 2012; published 23 Jul 2012

Similarly, it can be proved that $d\bar{I}_s / dz = 0$. Equations (1a) and (1b) are then rewritten as follows:

$$\frac{dG_p}{dz} = -\alpha - 2g_R \frac{\lambda_s}{\lambda_p}\sqrt{\bar{I}_s}\cosh(G_s) \tag{18}$$

$$\frac{dG_s}{dz} = -\alpha + 2g_R \sqrt{\bar{I}_p}\cosh(G_p) \tag{19}$$

The boundary conditions in Eq. (2) are also rewritten in terms of $\bar{I}_{p,s}$ and $G_{p,s}(z)$, i.e.,

$$\begin{aligned} G_p(0) &= \ln\frac{I_{in}(1-R_{pl}) + \sqrt{I_{in}^2(1-R_{pl})^2 + 4R_{pl}\bar{I}_p}}{2\sqrt{\bar{I}_p}} \\ G_p(L) &= \frac{1}{2}\ln\frac{1}{R_{pr}}, G_s(0) = -\frac{1}{2}\ln\frac{1}{R_{sl}}, G_s(L) = \frac{1}{2}\ln\frac{1}{R_{sr}}. \end{aligned} \tag{20}$$

The steady-state conditions for the pump and the Stokes waves can be acquired by integrating Eqs. (18) and (19):

$$G_p(0) = \delta_p + g_R \frac{\lambda_s}{\lambda_p}\int_0^L [2\sqrt{\bar{I}_s}\cosh(G_s)]dz, \tag{21}$$

$$g_R \int_0^L [2\sqrt{\bar{I}_p}\cosh(G_p)]dz = \delta_s. \tag{22}$$

Below or at threshold, i.e., $I_{in} \le I_{th}$, $\sqrt{\bar{I}_s} = 0$, the pump gain factor can be obtained from Eqs. (18) and (21):

$$G_p(z) = \delta_p - \alpha z. \tag{23}$$

From the first boundary condition in Eq. (20),

$$\sqrt{\bar{I}_p} = \frac{I_{in}(1-R_{pl})}{\exp(\delta_p) - R_{pl}\exp(-\delta_p)}. \tag{24}$$

Under the assumption that $G_p(z)$ is linearly dependent on z, the integration in Eq. (22) can be approximated as

$$\int_0^L \cosh[G_p(z)]dz = L\frac{\sinh[G_p(z)] - \sinh[G_p(0)]}{G_p(L) - G_p(0)} = L_p(z). \tag{25}$$

At or above threshold, i.e., $I_{in} \ge I_{th}$, Eqs. (22) and (25) yield:

$$\delta_s = 2g_R\sqrt{\bar{I}_p}L_p(L). \tag{26}$$

when $I_{in} = I_{th}$, the mean pump intensity $\bar{I}_p^{1/2}$ must satisfy both Eqs. (24) and (26), i.e.,

$$\sqrt{\bar{I}_p} = \frac{I_{th}(1-R_{pl})}{\exp(\delta_p) - R_{pl}\exp(-\delta_p)} = \frac{\delta_s}{2g_R L_p(L)}. \tag{27}$$

The threshold intensity in Eq. (4) is then solved from Eq. (27).

#166138 - $15.00 USD Received 5 Apr 2012; revised 15 Jun 2012; accepted 13 Jul 2012; published 23 Jul 2012